Article

Cell Host & Microbe

Phosphatidic Acid-Mediated Signaling Regulates Microneme Secretion in *Toxoplasma*

Graphical Abstract

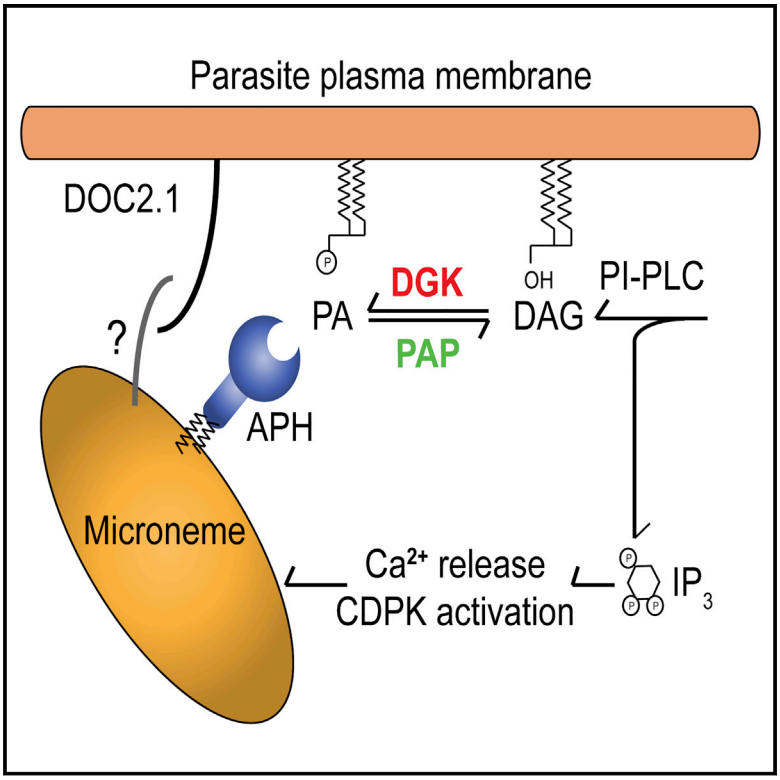

Authors

Hayley E. Bullen, Yonggen Jia, Yoshiki Yamaryo-Botté, ..., Vern Carruthers, Cyrille Y. Botté, Dominique Soldati-Favre

Correspondence

dominique.soldati-favre@unige.ch

In Brief

Microneme secretion is essential for efficient propagation of Apicomplexan parasites. In this issue of *Cell Host & Microbe*, Bullen et al. (2016) demonstrate that this process is underpinned by phosphatidic acid regulation at the parasite plasma membrane, controlled by the essential enzyme DGK1 and sensed by the microneme protein APH.

Highlights

- Membrane phosphatidic acid (PA) regulation is linked to *T. gondii* microneme secretion
- Diacylglycerol kinase-1 (DGK1) underpins PA generation for microneme secretion
- The microneme surface protein APH detects PA at the parasite plasma membrane
- Both APH and DGK1 are critical for microneme secretion in *T. gondii*

Bullen et al., 2016, Cell Host & Microbe *19*, 349–360
March 9, 2016
http://dx.doi.org/10.1016/j.chom.2016.02.006

Cell Host & Microbe
Article

Phosphatidic Acid-Mediated Signaling Regulates Microneme Secretion in *Toxoplasma*

Hayley E. Bullen,[1,4] Yonggen Jia,[1,4] Yoshiki Yamaryo-Botté,[2] Hugo Bisio,[1] Ou Zhang,[3] Natacha Klages Jemelin,[1] Jean-Baptiste Marq,[1] Vern Carruthers,[3] Cyrille Y. Botté,[2] and Dominique Soldati-Favre[1,*]
[1]Department of Microbiology and Molecular Medicine, CMU, University of Geneva, 1 Rue Michel-Servet, CH-1211 Geneva 4, Switzerland
[2]Apicolipid group, Institut Albert Bonniot UMR5309, CNRS, Université Grenoble Alpes, INSERM, Domaine de la Merci, 38700, La Tronche, France
[3]Department of Microbiology and Immunology, University of Michigan Medical School, 1150 14 W. Medical Center Dr., Ann Arbor, MI 48109-5620, USA
[4]Co-first author
*Correspondence: dominique.soldati-favre@unige.ch
http://dx.doi.org/10.1016/j.chom.2016.02.006

SUMMARY

The obligate intracellular lifestyle of apicomplexan parasites necessitates an invasive phase underpinned by timely and spatially controlled secretion of apical organelles termed micronemes. In *Toxoplasma gondii*, extracellular potassium levels and other stimuli trigger a signaling cascade culminating in phosphoinositide-phospholipase C (PLC) activation, which generates the second messengers diacylglycerol (DAG) and IP_3 and ultimately results in microneme secretion. Here we show that a delicate balance between DAG and its downstream product, phosphatidic acid (PA), is essential for controlling microneme release. Governing this balance is the apicomplexan-specific DAG-kinase-1, which interconverts PA and DAG, and whose depletion impairs egress and causes parasite death. Additionally, we identify an acylated pleckstrin-homology (PH) domain-containing protein (APH) on the microneme surface that senses PA during microneme secretion and is necessary for microneme exocytosis. As APH is conserved in Apicomplexa, these findings highlight a potentially widely used mechanism in which key lipid mediators regulate microneme exocytosis.

INTRODUCTION

Active host cell entry is an essential step in the propagation of obligate intracellular parasitism by apicomplexan parasites, members of which include the major etiologic agents of malaria (*Plasmodium spp.*) and toxoplasmosis (*Toxoplasma gondii*). Underpinning this process is the release of apical secretory organelles termed micronemes, secretion of which is a prerequisite for gliding motility, invasion, and egress from infected cells (reviewed in Sharma and Chitnis, 2013). Despite its central role in infectivity, our current understanding of the molecular mechanisms governing microneme secretion is sparse. Microneme exocytosis is known to follow changes in extracellular potassium levels (Singh et al., 2010), implicates cyclic GMP-dependent protein kinase G (PKG) (Brochet et al., 2014) and phosphoinositide regulation (Brochet et al., 2014), and responds to an increase in intracellular calcium concentration (Brochet et al., 2014; Garg et al., 2013; Singh et al., 2010; Singh and Chitnis, 2012; Wiersma et al., 2004). PKG activity promotes formation of the phosphoinositide-phospholipase C (PI-PLC) substrate $PI_{(4,5)}P_2$ (Brochet et al., 2014), implicating PI-PLC as the downstream mediator of PKG activity. Concordantly, *P. falciparum* PI-PLC transcription is upregulated during late blood stages, and the *P. berghei* homolog is refractory to genetic deletion (Raabe et al., 2011). Inhibitor studies suggest that PI-PLC acts on $PI_{(4,5)}P_2$ to generate the second messengers IP_3 and DAG and stimulates Ca^{2+} release from the endoplasmic reticulum (ER) or other internal stores (Singh et al., 2010) through unidentified receptors (reviewed in Budu and Garcia, 2012). Ethanol stimulation of *T. gondii* microneme secretion also triggers an increase in calcium, likely as a result of PI-PLC-derived IP_3 (Carruthers et al., 1999; Lovett et al., 2002). Members of the calcium-dependent protein kinase (CDPK) family are critically involved downstream of this signaling cascade (Garrison et al., 2012; Lourido et al., 2012; McCoy et al., 2012; reviewed in (Holder et al., 2012). Ultimately, a fusion event believed to involve SNARE-like proteins such as DOC2.1 (Farrell et al., 2012; Jean et al., 2014) enacts microneme exocytosis.

With a view to better deciphering microneme exocytosis, we have focused here on diacylglycerol (DAG) and phosphatidic acid (PA), downstream products of PI-PLC signaling at the parasite plasma membrane (PPM). DAG is interconverted to PA via DAG kinases (DGKs) and PA phosphatases (PAPs). In mammalian systems, PA is involved in signal transduction (Chasserot-Golaz et al., 2010), membrane dynamics (Kooijman et al., 2003), and exocytosis (reviewed in Ammar et al., 2013; Chasserot-Golaz et al., 2010), thus providing a precedent for PA to also play a role in microneme exocytosis in the Apicomplexa. We have identified and functionally characterized both the enzyme mediator of PA production and the corresponding PA-sensor underpinning an essential mechanism of microneme exocytosis conserved across the Apicomplexa.

RESULTS AND DISCUSSION

Modulation of PA Levels Plays a Critical Role in *T. gondii* Microneme Secretion

The importance of PA signaling in microneme secretion was implicated by the putative increase in its precursor (DAG) during

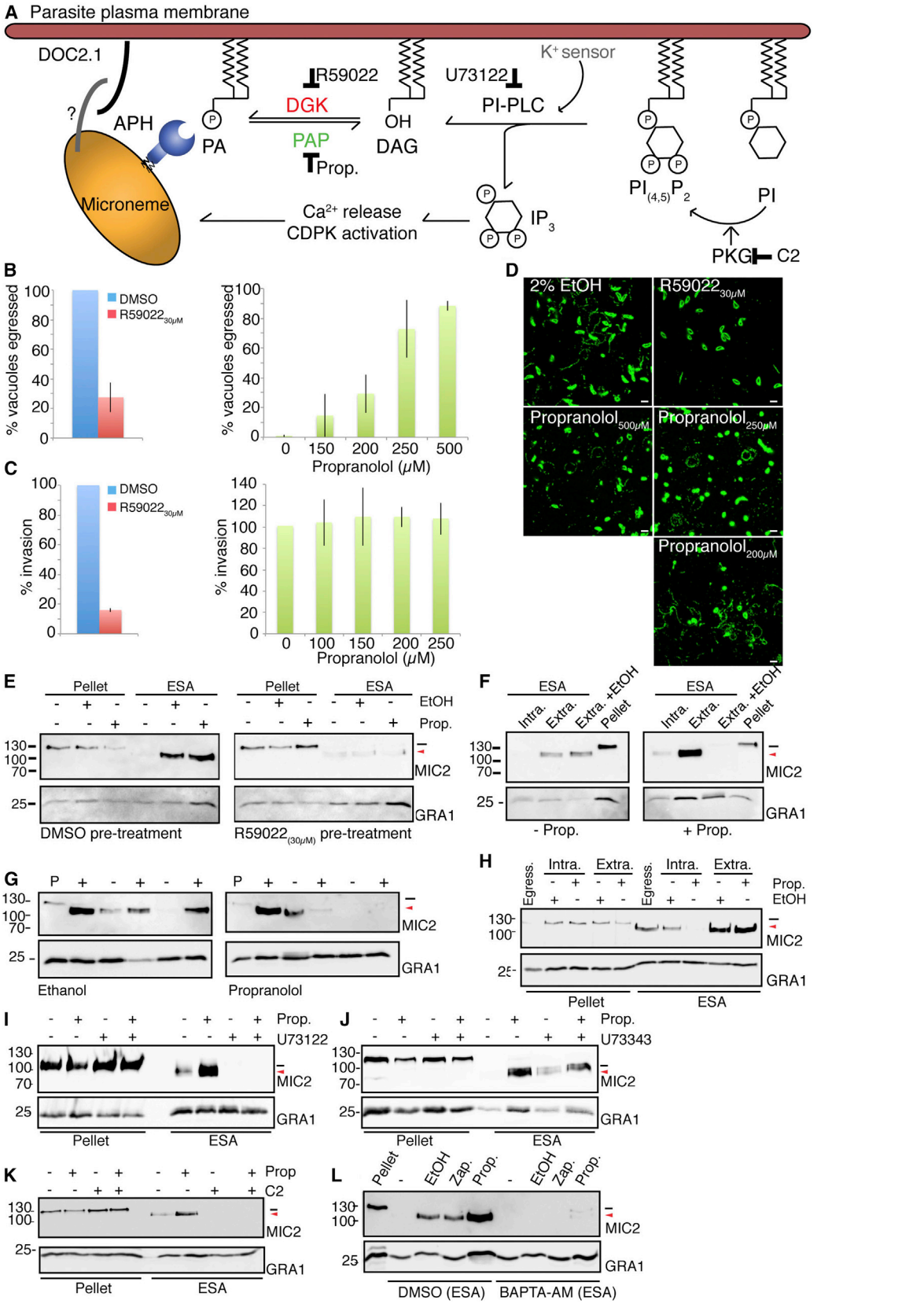

(legend on next page)

PI-PLC signaling (Figure 1A). The localization of PA-generating enzymes precludes the involvement of phospholipase D (mitochondrial, http://www.toxodb.org/toxo/) or lysophosphatidic acid acyltransferase (ER) (Lindner et al., 2014), solely implicating DGKs as priority candidates for generation of PA at the PPM (Figures 1A and S1A–S1C).

We first utilized commercially available DGK (R59022) (de Chaffoy de Courcelles et al., 1985) and PAP inhibitors (propranolol) (Baron and Malhotra, 2002) to probe this pathway, hypothesizing that blocking PA production would hamper microneme secretion, while blocking PA conversion to DAG would enhance microneme secretion (Figure 1A). These inhibitors were used in parallel for egress (Figure 1B), invasion (Figure 1C), gliding (Figure 1D), and microneme secretion assays (Figures 1E–1L). As hypothesized, R59022 blocked parasite egress (Figure 1B), invasion (Figure 1C), gliding (Figure 1D), and microneme exocytosis (Figure 1E). Concordantly, promoting PA accumulation by blocking PAP-activity with propranolol stimulated parasite egress (Figure 1B), gliding motility (Figure 1D), and microneme secretion (Figures 1F–1L). Importantly, propranolol acts most significantly when used in a buffer mimicking extracellular potassium concentrations that enable basal microneme secretion in the absence of additional stimuli (Figures 1F/1H). These data suggest that for propranolol to effect microneme secretion, the parasite must already be ''primed'' whereby the remainder of the pathway (Figure 1A) is already underway; potassium stimulation leading to PI-PLC activity and the concurrent increase in DAG and IP_3 are necessary for propranolol functioning.

Ethanol has previously been linked to microneme secretion and has been proposed to act through stimulating PI-PLC activity (Carruthers et al., 1999; Lovett et al., 2002). Here we sought to compare the effects of microneme stimulation by propranolol versus ethanol by repeatedly and sequentially stimulating parasites with either 2% ethanol or 250 μM propranolol (Figure 1G). While parasites stimulated with ethanol underwent multiple rounds of secretion (Figure 1G, left panels), those stimulated with propranolol generated only one significant burst of secretion that appeared to completely deplete the micronemal contents (Figure 1G, right panels), implying that these two compounds have distinct mechanisms of action upon the microneme secretion pathway.

This was further validated through microneme secretion assays completed in buffer mimicking intracellular ionic conditions (Figure 1H). In such conditions, only ethanol stimulated microneme secretion, concordant with propranolol being effective only once the remainder of the pathway in Figure 1 is activated and thus PA is being produced. Furthermore, these data imply that unlike ethanol, propranolol cannot stimulate an increase in intracellular calcium levels to elicit microneme secretion. To confirm this, calcium-sensing GCaMP6-expressing tachyzoites (Borges-Pereira et al., 2015) were incubated in either intracellular or extracellular buffer; stimulated with calcium ionophore (A23187), ethanol, or propranolol; and calcium flux was subsequently monitored (Figure S1D; Movies S1, S2, S3, and S4). Under all conditions, both A23187 and ethanol stimulated an increase in intracellular (parasite) calcium, whereas propranolol had no effect under either condition (Figure S1D; Movies S1, S2, S3, and S4). These data confirm that unlike ethanol, propranolol does not elicit microneme secretion through increasing calcium levels.

Despite the significant effect of propranolol on microneme secretion, invasion efficiency of treated parasites remained unchanged (Figure 1C, right panel), which is not surprising in light of the gliding assays (Figure 1D). Parasite gliding utilizes proteins secreted from the micronemes and assays reveal that in the presence of propranolol, parasites are indeed stimulated to glide; however, gliding activity is altered in a propranolol-concentration-dependent manner. At the maximal concentration of propranolol used in this study (500 μM), gliding trails are predominantly single circles, suggesting that the parasites secrete their micronemes in one burst and can then no longer glide as their micronemal contents are depleted/exhausted, concordant with data shown in Figure 1G. Importantly, as the concentration of propranolol is decreased, parasites increase the amount and type of trails that they deposit (multiple overlapping circles/random trails) indicating that while microneme secretion is still occurring, these lower concentrations are not sufficient to fully deplete/exhaust the micronemal contents and instead revert the gliding phenotype back to that seen for parasites stimulated

Figure 1. Phosphatidic Acid Is Essential for Microneme Secretion

(A) PA accumulation at the parasite periphery promotes APH membrane binding and facilitates DOC2.1/SNARE binding for microneme secretion. PA: phosphatidic acid. DGK: diacylglycerol kinase. PAP: phosphatidic acid phosphatase. DAG: diacylglycerol. PI-PLC: phophoinositide phospholipase C. PKG: cGMP-dependent protein kinase. R59022: DGK inhibitor. Propranolol: PAP inhibitor. C2: Compound 2, PKG inhibitor. U73122: PI-PLC inhibitor.

(B) R59022 blocks parasite egress (left panel) while propranolol stimulates parasite egress (right panel). Error bars represent ±SD for 100 vacuoles counted in triplicate from three biological replicates.

(C) R59022 blocks parasite invasion of host cells (left panel), propranolol has no effect (right panel). Error bars represent ±SD for 100 vacuoles counted in triplicate from three biological replicates.

(D) Gliding motility is blocked by treatment with R59022 while propranolol stimulates gliding motility in a dose-dependent manner.

(E) Ethanol (EtOH, 2%) or propranolol (Prop., 500 μM) stimulation of microneme secretion is blocked by R59022 (30 μM, diminished levels of secreted MIC2 and AMA1). GRA1: control for parasite viability. ESA: excretory secretory antigens.

(F) Extracellular parasites were incubated sequentially in buffer mimicking intracellular (Intra.), extracellular (Extra.) or extracellular conditions with 2% EtOH (Extra. +EtOH) in the presence/absence of 500 μM propranolol (± Prop.). Propranolol completely depletes micronemal contents in extracellular buffer.

(G) Microneme secretion was sequentially turned on (+) and off (−) three times (left to right) with either 2% EtOH or 500 μM propranolol. MIC2 secretion can be repeatedly stimulated with ethanol, but propranolol triggers only one significant micronemal burst prior to microneme depletion. GRA1 labeling indicates that parasites remain alive following propranolol stimulation. P: pellet.

(H) Only ethanol (EtOH, 2%) and not propranolol (Prop., 500 μM) causes microneme secretion in buffer mimicking intracellular conditions (Intra.). Egress; unstimulated parasites in extracellular buffer.

(I–L) (I) U73122 (10 μM), (J) U73343 (10 μM), (K) Compound 2 (C2, 1 μM), and (L) BAPTA-AM (10 μM) treatment ablates propranolol-induced microneme secretion. −: Full length protein. Red arrowhead: Processed MIC. EtOH: 2% ethanol. Zap.: 500 μM Zaprinast. Prop.: 500 μM propranolol.

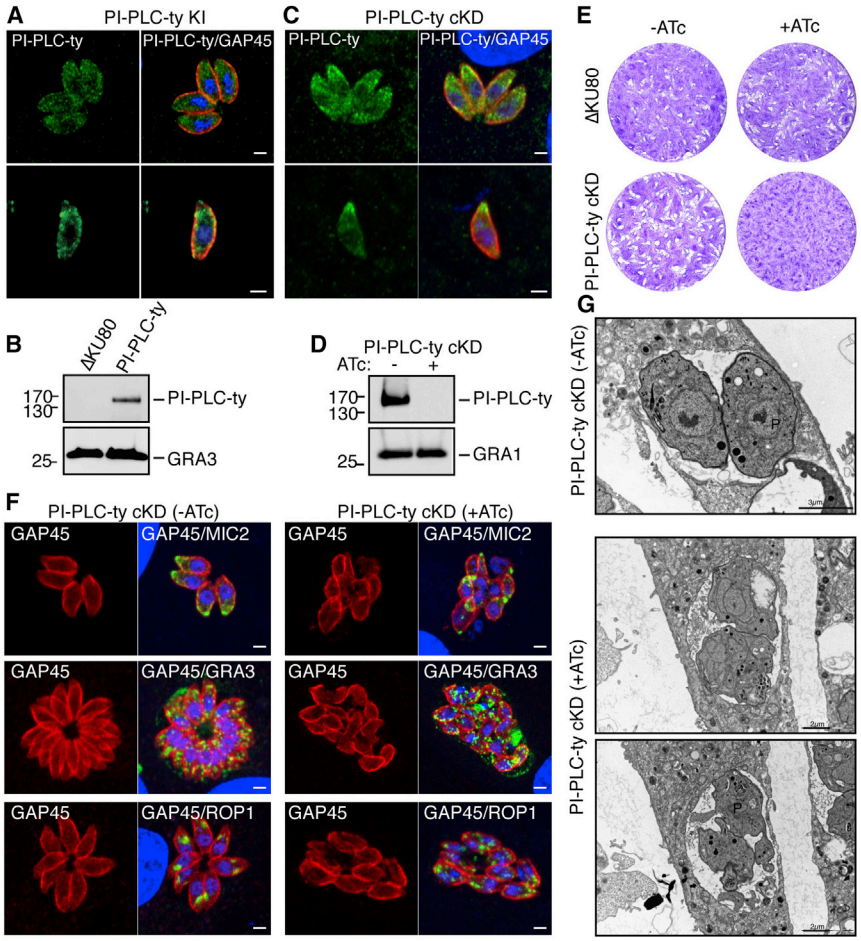

Figure 2. TgPI-PLC Is Crucial for Parasite Survival

(A and C) Endogenously C-terminally tagged TgPI-PLC (A) or TgPI-PLC cKD (C) localize to apical puncta and peripheral accumulations within intracellular parasites and cluster apically in extracellular parasites. GAP45: parasite periphery. Scale bar 2 μm.

(B) TgPI-PLC-ty migrates at the expected size on western blot (125kDa). GRA3: loading control.

(D) PI-PLC-ty cKD parasites are regulated by ATc in 48 hr. GRA1: loading control.

(E) PI-PLC-ty cKD but not parental ΔKU80 parasites display a severe growth defect in the absence of PI-PLC-ty (PI-PLC-ty cKD +ATc).

(F) IFA of PI-PLC-ty cKD parasites ± ATc (72hr). Parasite morphology is grossly affected following depletion of PI-PLC-ty. GAP45: parasite periphery. MIC2: micronemes. GRA3: dense granules. ROP1: rhoptries.

(G) Electron microscopy reveals gross morphological defects in PI-PLC-ty cKD parasites +ATc (bottom two panels) while PI-PLC-ty cKD parasites (−ATc) appear morphologically normal. P: parasite.

with ethanol (Figure 1D). In light of these data, it is not surprising that the invasion efficiency of propranolol treated parasites is not increased compared to untreated parasites.

Confirmation that propranolol impacts upon the pool of PA generated through the PI-PLC pathway (Figure 1A) was sought through use of various inhibitors including the DGK inhibitor (R59022, Figure 1E), PI-PLC inhibitor (U73122, Figure 1I), its inactive analog U73343 (Figure 1J), and PKG inhibitor Compound 2 (Figure 1K). These data revealed that blocking production of PA at any point along the pathway outlined in Figure 1A precludes propranolol activity and that it therefore acts upon a pool of PA upregulated during the microneme secretion-signaling pathway. Furthermore, pre-treatment of parasites with a chelator of intracellular calcium (BAPTA-AM, Figure 1L) blocked ethanol, zaprinast (a phosphodiesterase inhibitor), and propranolol-stimulated microneme secretion, confirming that the production of PA alone cannot override the requirement for a rise in intracellular calcium during this process (Figure 1L). These data are in complete agreement with the primary propranolol secretion assays (Figures 1F/1H) and highlight the importance of both arms of the pathway (Figure 1A) running concurrently to enact efficient microneme secretion. Overall, these data highlight the importance of a delicate balance between DAG and PA levels during microneme exocytosis.

PI-PLC Is Essential for Lytic Stage Growth

The signaling pathway outlined in Figure 1A strongly implicates the importance of PI-PLC in generating both IP_3 and DAG to underpin efficient microneme exocytosis. As such, we appended 3ty-tags to the endogenous C terminus of *Tgpiplc* (Figures 2A–2D and S2A/S2B) to confirm its localization by indirect immunofluorescence assay (IFA). Previous reports utilized a peptide antibody to localize PI-PLC to the parasite periphery (Fang et al., 2006); however, we detected endogenous PI-PLC both in the parasite cytosol and in peripheral and apical accumulations (Figures 2A/2C). Importantly, PI-PLC-ty appeared to cluster at the parasite apex in extracellular parasites (Figures 2A/2C, bottom panels), concordant with it playing a role in microneme exocytosis. The dual localization of PI-PLC-ty does however suggest that PI-PLC likely plays multiple roles in lipid regulation and does not act exclusively for PPM lipid regulation/microneme exocytosis.

Attempts to knockout *Tgpiplc* were unsuccessful, and we therefore generated a Tet-inducible knockdown (PI-PLC-ty cKD) that efficiently regulated PI-PLC-ty expression upon addition of anhydrotetracycline (ATc) (Figures 2C–2G and S2C/S2D). Plaque assays clearly demonstrated a significant impact on lytic stage growth in the absence of PI-PLC (Figure 2E), concordant with PI-PLC playing an essential role within the parasite. Importantly, PI-PLC depletion caused significant morphological abnormalities whereby rosette formation was perturbed and nuclear material was seen within the parasitophorous vacuole (Figures 2F/2G). This severe phenotype precluded the completion of assays specifically investigating the role of PI-PLC in microneme exocytosis, yet implicated PI-PLC in a vast and as yet incompletely understood signaling cascade.

TgDGK1 Is Essential for Lytic Stage Growth

The effects of both R59022 and propranolol on microneme secretion, combined with the severe deleterious phenotype we observed upon PI-PLC depletion, strongly implicated the presence of a pool of PA at the parasite periphery. Consequently, to confirm that these inhibitors were indeed acting upon a pool of PPM-associated PA, we utilized a yeast-derived molecular probe that binds PA (Spo20pGFP$_{wt}$) or its inactive form that does not bind PA (Spo20pGFP$_{mut}$) (Nakanishi et al., 2004) by IFA (Figures 3A/3B). Spo20pGFP$_{wt}$ but not Spo20pGFP$_{mut}$ specifically labels the parasite periphery (Figure 3A); however, this peripheral localization is abolished by addition of R59022, whereupon Spo20pGFP$_{wt}$ re-localizes to the cytosol (Figure 3B, bottom panels) confirming both the specificity of Spo20pGFP$_{wt}$ in vivo and the activity of R59022 toward a plasma membrane DGK to block PA production.

Three genes were found to encode putative DGKs in the *T. gondii* genome (*Tgdgk1*, ToxoDB: TGME49_202460; *Tgdgk2*, ToxoDB: TGME49_259830; and *Tgdgk3*, ToxoDB: TGME49_239250), but only *Tgdgk1* and *Tgdgk3* are conserved across the Apicomplexan phylum (Figure S1A). Only TgDGK1 localizes to the parasite periphery (Figures 3C and S1A), concordant with a role in peripheral PA generation. Furthermore, TgDGK2 (dense granule/PV localization, Figure S1A) and TgDGK3 (microneme localization, Figure S1A) were found to be dispensable for parasite survival (data not shown) while *Tgdgk1* was refractory to genetic deletion, and conditional knockdown strategies were implemented. A Tet-inducible knockdown (myc-DGK1cKD) efficiently turned off *Tgdgk1* expression upon addition of ATc (Figures 3D/3E/3F/3G/3H/3I and S2G–S2L), and plaque assays clearly demonstrated that myc-DGK1 depletion severely impacted the parasite lytic cycle (Figure 3E; IFA, Figure 3F). Electron microscopy (Figure 3G) revealed half-empty vacuoles indicative of parasite lysis. The apical positioning of the micronemes was perturbed upon DGK1 depletion as indicated by both apical and posterior MIC2 labeling (Figure 3F, top right panel), while the remainder of the organelles investigated (mitochondrion, apicoplast, rhoptries, Figures S2I–S2K) localized correctly when the myc-DGK1-depleted parasites remained intact. We believe that dispersal of the micronemes in myc-DGK1-depleted parasites is likely a result of parasite death rather than any direct impact of myc-DGK1 on the positioning of the micronemes themselves. As such, the appearance of the glycosylphosphatidylinositol (GPI) anchored plasma membrane protein SAG1 within the vacuole space was highly suggestive of extensive parasite lysis with PPM destruction (Figure 3F). In addition, membranous material seen in the "parasite-depleted" vacuoles potentially constitutes a mixture of dead parasites and remnants of the intravacuolar nanotubular network (Figures 3F and 3G). Spo20pGFP$_{wt/mut}$ localization within myc-DGK1cKD parasites demonstrated that in the absence of myc-DGK1 (myc-DGK1cKD +ATc), Spo20pGFP$_{wt}$ relocates to the nucleus/cytosol, indicating that myc-DGK1 is the most likely regulator of PA at the PPM (Figure 3H).

To confirm that these data are indeed due to DGK1 regulation of PA, we quantified the PA in myc-DGK1cKD parasites via gas chromatography-mass spectrometry (GC-MS) after lipid separation with high-performance thin-layer chromatography. When myc-DGK1 is depleted (Figure 3I, +ATc; blue), PA was 10%–40% lower than the parental control (Figure 3I, −ATc; red). Furthermore and concordant with our previous findings, we determined that PA levels are also reduced in R59022-treated parasites (Figure 3J, blue) to a level similar to that seen for myc-DGK1-depleted parasites. While we were able to detect changes in PA levels, these changes were minute, and the total amount of PA in the parasites was subject to large variation between samples (Figures 3I/3J). These fluctuations are likely due to the central and versatile role of PA as both a major phospholipid precursor and a strong signal transducer in eukaryotic cells (Botté et al., 2012; Chasserot-Golaz et al., 2010). The precise origin and role of the total pool of PA in *T. gondii* is yet to be determined, and such a small decrease in total PA suggests that DGK1 is likely not responsible for the bulk synthesis of PA and is indeed more likely to be serving transient PA synthesis for lipid signaling at the PPM.

Given that these data confirm that DGK1 is involved in PA synthesis at the parasite periphery, we developed an alternative and more synchronized way to deplete TgDGK1 via a fusion with a destabilization domain (DD) (Herm-Götz et al., 2007). To ensure that the N-terminal DD fusion did not impact upon DGK1 function, we first complemented the myc-DGK1cKD strain with an N-terminally DD/HA-tagged copy of TgDGK1 regulated by Shld-1 (myc-DGK1cKD (Comp. DD/HA-DGK1cKD); Figures S2N–S2P). Expression of DD/HA-DGK1 in the absence of myc-DGK1 (+Shld-1/+ATc) rescued parasite fitness (Figure S2N), demonstrating that the phenotype described for myc-DGK1cKD was indeed due to myc-DGK1 depletion and also that the DD fusion does not interfere with DGK1 function. As expected, DD/HA-DGK1 localized to the parasite periphery (Figure S2O), and western blot analyses confirmed that myc-DGK1cKD was still regulated by ATc in the complemented strain (Figure S2P).

Next we generated a parasite line expressing endogenously N-terminally tagged DDmyc-DGK1cKD stabilized by Shld-1 (Sidik et al., 2014). Plaque assays of DDmyc-DGK1cKD minus Shld-1 reconfirmed the importance of TgDGK1 for parasite survival (Figure 3K), and IFAs showed that destabilization of the protein recapitulated the phenotype observed for the myc-DGK1cKD strain +ATc (Figure 3L). Rather unexpectedly, the loss of parasite integrity also took time to manifest following shld-1 removal, suggesting that the phenotype, likely due to a detrimental imbalance of PA/DAG, takes time to build up (Figure 3L, −Shld-1). In parasites with only a marginal loss in membrane integrity, a gradual and significant impact of DGK1-destabilization on induced egress was noted (Figure 3M), and microneme secretion at these time points was also impaired (Figure 3N). Overall, these data clearly demonstrate the importance of PA generation by DGK1 to enact microneme secretion in *T. gondii*.

APH Acts as a PA Sensor and Is Essential for Microneme Secretion

Given that PA levels clearly impact microneme exocytosis, we sought to identify the protein sensor of PA at the parasite membrane. We completed bioinformatics searches in ToxoDB and PlasmoDB for pleckstrin homology (PH)-domain-containing proteins, as these domains are known to bind phosphoinositides. We found 14 genes containing predicted PH-domains in *T. gondii* and seven genes in *Plasmodium* (Table S1); however, only one gene was conserved across all Apicomplexa

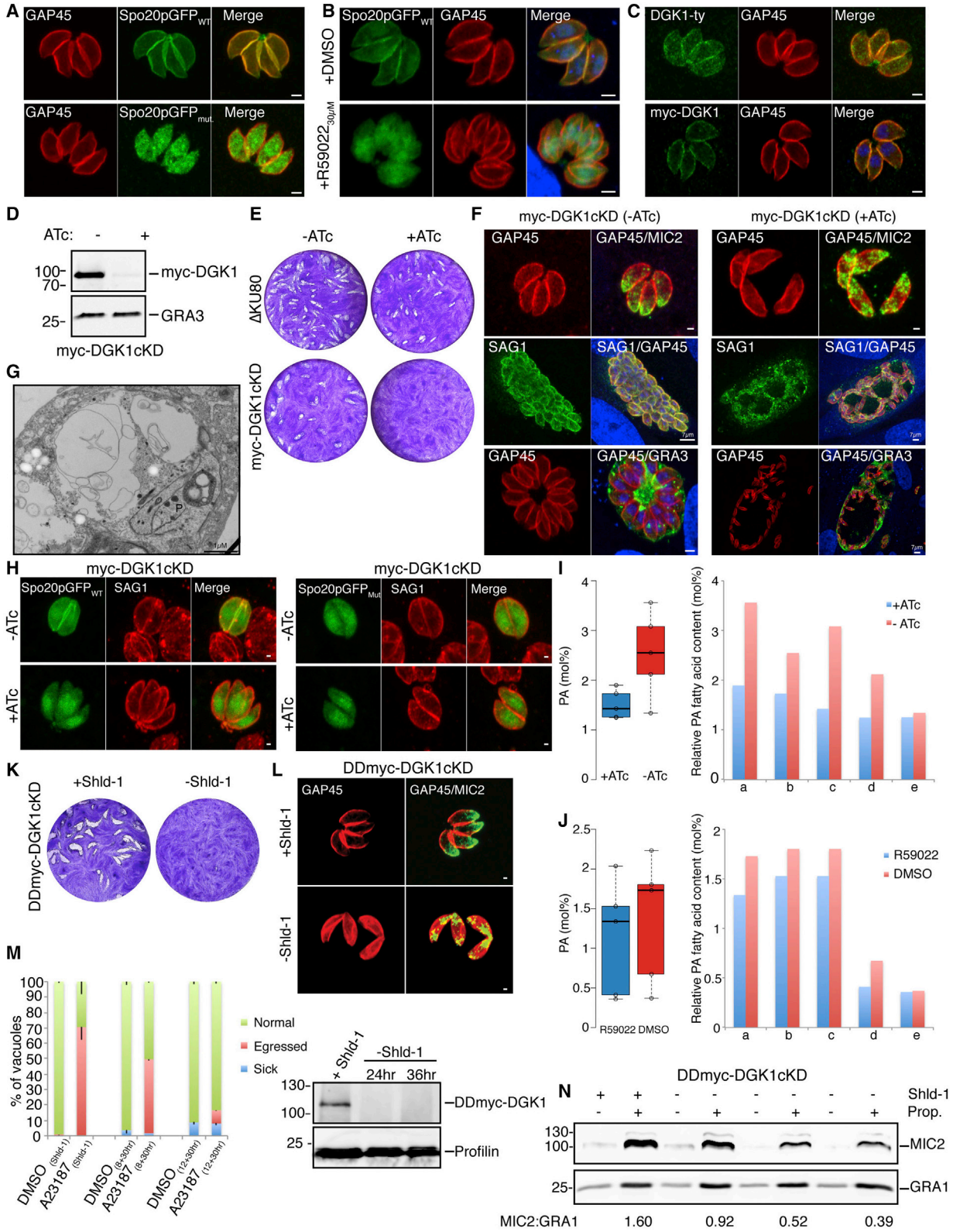

Figure 3. TgDGK1 Is Crucial for Parasite Survival

(A) Marker of PA (Spo20pGFP$_{WT}$) but not its inactive form (Spo20pGFP$_{mut}$) labels PA at the parasite periphery alongside GAP45.

(B) Treatment of Spo20pGFP$_{WT}$ parasites with DGK-inhibitor R59022 ablates membrane localization.

(legend continued on next page)

(ToxoDB: TGME49_249970), and it is this gene that formed the basis of our analysis (Figure S3). In addition to a PH domain, the protein encoded by TGME49_249970 possesses an N-terminal stretch of 21 highly conserved residues with strong predictions for the presence of myristoylation (G2) and palmitoylation (C7) motifs (Figures 4A–4C, S3A, and S3B). We termed this protein "APH" (acylated pleckstrin-homology domain) and revealed its localization to the micronemes with specific anti-APH antibodies (Figure 4A, top panel). This localization was confirmed by generation of transgenic parasites expressing a ty-tagged second-copy (TgAPH-ty) (Figure 4A middle panel, Figures S3C and S3D). In addition, a fusion of the conserved N-terminal 21 residues of TgAPH to mCherry (N21-APH-mCh) localized to the micronemes (Figure 4A bottom panel), and mutation of the putative acylation motifs (G2A or C7A) caused APH to redistribute throughout the parasite cytosol (Figure 4B). Overall, these data imply that APH is trafficked to the micronemes via palmitoylation/myristoylation within the first N-terminal 21 residues. Concordantly and as expected for a myristoylated/palmitoylated protein, TgAPH-ty was found to be insoluble in PBS and fully soluble in 1% Triton X-100 (Figure 4C, left panel). In contrast, TgAPH myristoylation (G2A) and palmitoylation (C7A) mutants were found to be readily soluble in PBS (Figure 4C, right panels). Lastly and consistent with acylation, protease protection assays confirmed that APH is localized to the outer micronemal surface (Figure 4D). It should be noted that all apicomplexan parasites possess micronemes and contain a highly conserved *aph* gene (Figure S3B) and thus are all likely to utilize this protein for the same role.

Confirmation that TgAPH binds PA was sought through both phosphoinositide-strip (PIP-strip) and liposome-binding assays (Figures 4E–4G and S3E). PIP-strips established that bacterially produced TgAPH and the PH-domain alone, the orthologous *Plasmodium falciparum* protein (PfAPH) and the yeast $Spo20p_{WT/Mut}$ proteins bind strikingly to PA and not as intensely to any other phosphoinositides (Figure 4E). In these assays an excess of protein is overlaid upon on an excess of lipid (100 pmol/spot); thus, we were unable to distinguish binding of the $Spo20p_{WT/Mut}$ to PA in vitro despite its clear specificity in vivo. We were however able to validate these results for APH via liposome binding assays, wherein the specificity of TgAPH, the PH-domain, and PfAPH binding to PA was confirmed and shown to be statistically significant (Figures 4F and 4G). To further strengthen this data and assess directly how APH responds to changes in PA levels, we expressed a non-acylated, soluble form of APH by N-terminal fusion with DD (DDmyc-APH) and investigated its localization upon propranolol treatment (Figures 4H/4I). DDmyc-APH was found to re-localize to the parasite apex upon propranolol treatment, concordant with it binding to PA. This effect was ablated in the presence of DGK-inhibitor R59022 (Figure 4H), indicating that DDmyc-APH responds to the pool of PA produced specifically by DGK1 and enhanced by propranolol treatment.

Being refractory to genetic deletion, *Tgaph* was instead deleted by a gene excision strategy utilizing the rapamycin-dependent, dimerizable Cre-recombinase (Andenmatten et al., 2013) (Figures S3F–S3H). Following addition of rapamycin, loss of *Tgaph* expression was seen in 10%–20% of the population (Figure 5A, top panel). We were unable to clone any excised parasites, thus formally confirming that the *Tgaph* gene is essential. Within this system, removal of TgAPH did not alter microneme biogenesis, localization (Figure 5A, bottom panel), or intracellular growth (Figure S3H); however, concordant with a role in microneme secretion, *Tgaph*-excised parasites (ty-APH-cKO) displayed a marked block in invasion (Figure 5B) and egress (Figure 5C). The low excision rate precluded quantitative assessment of microneme secretion; therefore, we generated an additional conditional knockdown line both for completion of microneme secretion assays and also to confirm the data from the DiCre strain. As such, we generated an ATc-regulatable conditional knockdown of *Tgaph* (ty-APH-cKD) (Figures S3I–S3K).

(C) Endogenously C- (top) or N-terminally (bottom) tagged *Tgdgk1* localizes to the parasite periphery. Scale bar 2μm.

(D) myc-DGK1cKD parasites are regulated by ATc in 48 hr. GRA3: loading control.

(E) myc-DGK1cKD but not parental ΔKU80 parasites display a severe growth defect in the absence of mycDGK1 (myc-DGK1cKD +ATc).

(F) IFA of myc-DGK1cKD parasites ± ATc (48–96 hr). Upon myc-DGK1 removal, a pool of MIC2 mis-localizes to the parasite posterior (top right), the PPM degrades (SAG1, middle right), and rosette formation is perturbed (GRA3, bottom right). SAG1: PPM. GRA3: dense granule. Scale bar 2μm unless otherwise stated.

(G) Electron micrograph of myc-DGK1cKD +ATc/72 hr. Parasite morphology is severely perturbed, and membranous whorls are seen within the vacuolar space. P: parasite.

(H) mycDGK1cKD parasites transiently transfected with constructs expressing DDmycSpo20pGFP_WT ($Spo20pGFP_{WT}$) or DDmycSpo20pGFP_Mut ($Spo20pGFP_{Mut}$) were treated with Shld-1 ± ATc. In the absence of DGK1 (+ATc) $Spo20pGFP_{WT}$ translocates from the parasite periphery to the cytosol. There is no change in $Spo20pGFP_{Mut}$ localization either ± ATc. Scale bar 2 μm.

(I) Total lipid was extracted from myc-DGK1cKD parasites grown in the presence (+ATc) or absence (−ATc) of ATc. PA was separated from total lipid by HPTLC, quantified by GC-MS, normalized according to cell number, and shown relative to total fatty acid content (mol%). In myc-DGK1cKD parasites, the addition of ATc induced a decrease in PA (+ATc).

(J) Similarly, the addition of DGK-inhibitor R59022 (30 μM) induced a decrease in PA in comparison to its control (DMSO). For both (I) and (J), box plot center lines show the median (+ATc, 1.43; −ATc, 2.55; R50922, 1.34; DMSO, 1.72); box limits: 25^{th} and 75^{th} percentiles. Interquartile range: +ATc, 0.47; −ATc, 0.96; R50922, 1.12; DMSO, 1.13. Whiskers; range of values (+ATc, 1.25–1.90; −ATc, 1.34–3.56; R50922, 0.36–2.04; DMSO, 0.36–2.23). Outliers represented by dots. n = 5 sample points. a–e represent individual biological replicates for each assay condition.

(K) DDmyc-DGK1cKD parasites display a severe growth defect in the absence of DDmycDGK1 (DDmyc-DGK1cKD −Shld-1).

(L) IFA of DDmyc-DGK1cKD parasites ± Shld-1 reflect the same lytic defect seen in myc-DGK1cKD parasites. MIC2: micronemes. GAP45: parasite periphery. Scale bar: 1 μm.

(M) Egress assay of DDmyc-DGK1cKD parasites grown −Shld-1 for either 8 (8 + 30 hr) or 12 (12 + 30 hr) hr prior to a further 30 hr growth on new monolayers (−Shld-1) to deplete DDmyc-DGK1. Vacuoles were scored by IFA as normal, egressed or sick (DGK1-depleted, lysed parasites). DGK1 depletion abrogated parasite egress. (Right) Western blot control for DDmyc-DGK1cKD depletion. Error bars represent ±SD for 100 vacuoles counted in triplicate from three biological replicates.

(N) Microneme secretion is reduced in the absence of DDmyc-DGK1 as indicated by reduced MIC secretion quantified as a ratio of MIC2:GRA1 signal. GRA1: loading control.

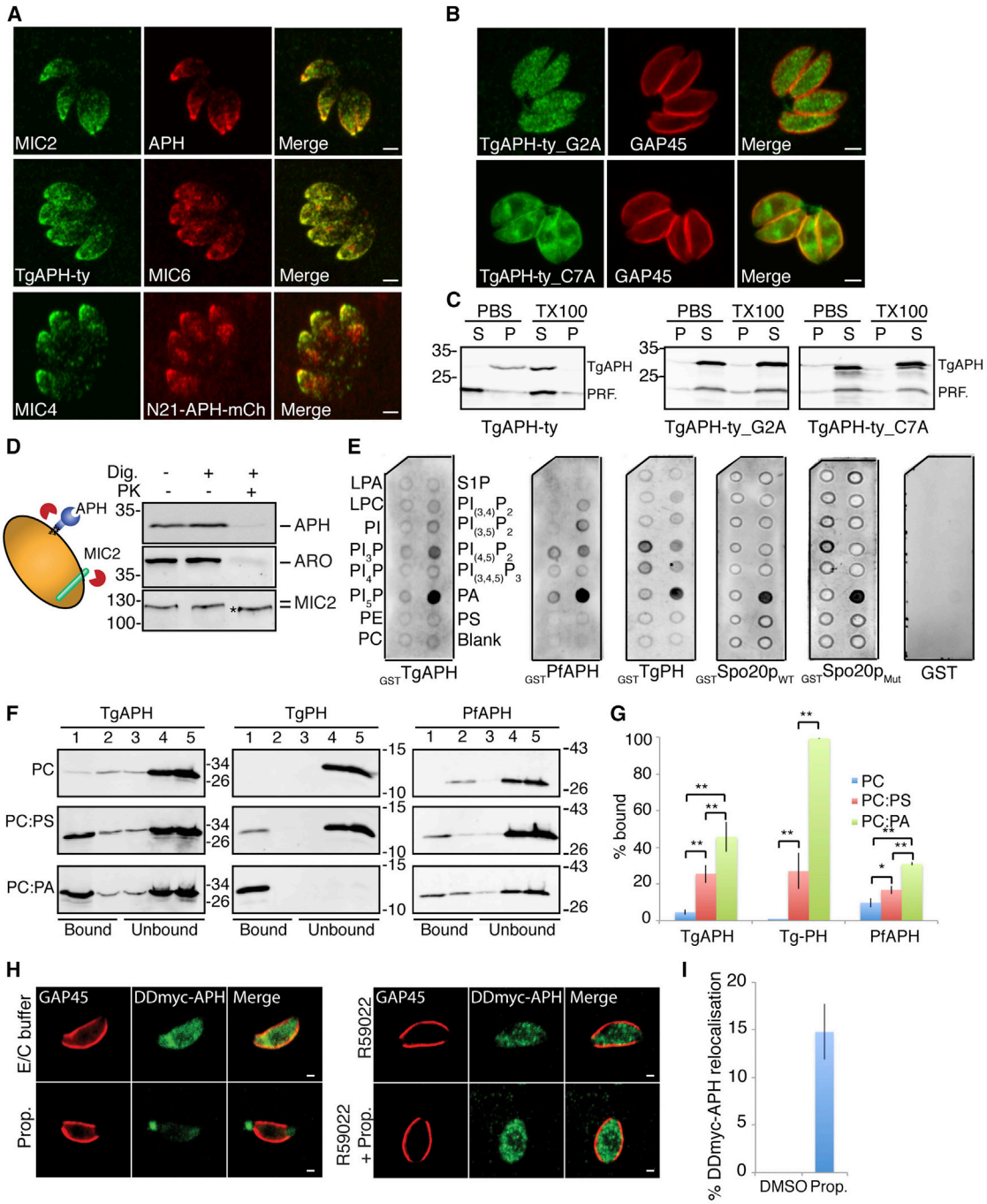

Figure 4. APH Localizes to the Micronemes and Binds PA

(A) Endogenous TgAPH (top) and TgAPH-ty (middle) localize to the micronemes. The N-terminal 21 residues of TgAPH are sufficient for microneme targeting (N21-APH-mCh). MIC2/4/6: microneme markers.

(B) Mutating the putative myristoylation (TgAPH-ty_G2A, top panel) or palmitoylation motif (TgAPH-ty_C7A, bottom panels) ablates microneme localization. GAP45; parasite periphery.

(C) Parasites were solubilized in either PBS or 1%Triton X-100 (TX100) and split into soluble (S) and pellet (P) fractions. APH is PBS insoluble, while G2A and C7A mutants are PBS soluble.

(D) Digitonin (Dig.) permeabilization facilitates TgAPH digestion by proteinase K (PK). TgARO; rhoptry surface protein. MIC2 band shift (*) represents cleavage of small external portion.

(E) PIP-strip assays show specific $_{GST}$TgAPH/$_{GST}$PfAPH/$_{GST}$TgPH/$_{GST}$Spo20p$_{WT/Mut}$ PA binding. LPA: lysophosphatidic acid. LPC: lysophosphocholine. PE: phosphatidylethanolamine. PC: phosphatidylcholine. S1P: Sphingosine-1-phosphate. PS: phosphatidylserine.

(F) Immunoblots of recombinant TgAPH, the PH domain alone, or PfAPH-associated with liposomes. Recombinant proteins were incubated with liposomes containing phosphatidylcholine (PC), PC:phosphatidylserine (PS) (1:1 molar ratio) or phosphatidic acid (PA):PC (1:1 molar ratio). Fractions 1 and 2 represent

(legend continued on next page)

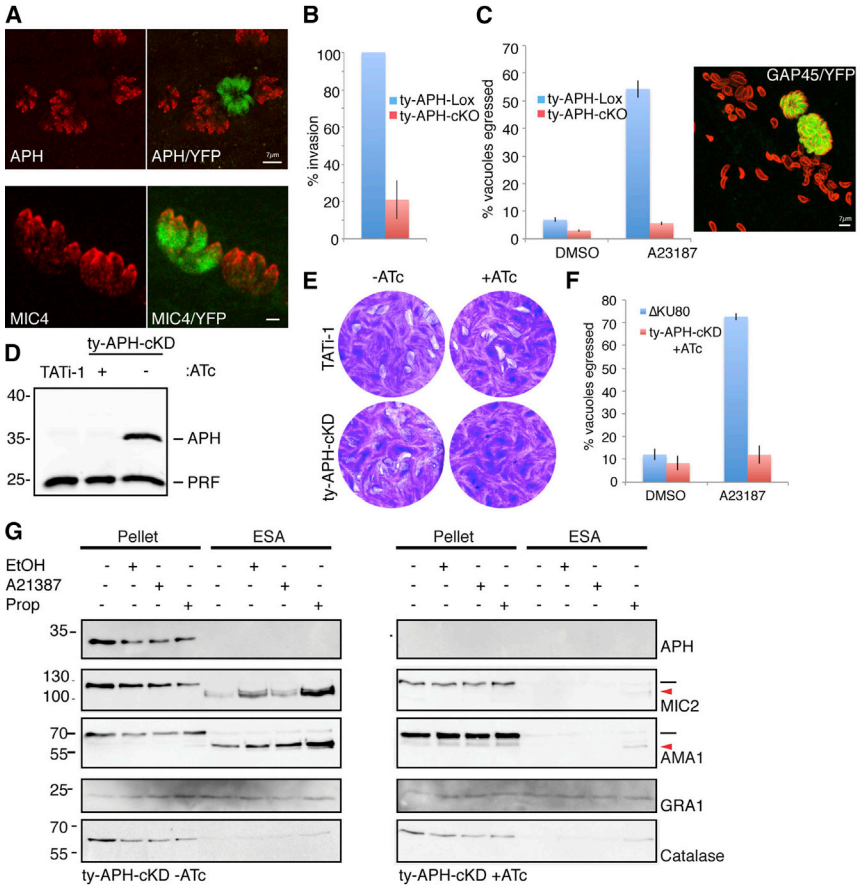

Figure 5. TgAPH Is Crucial for Microneme Secretion, Egress and Invasion

(A) Top: IFAs probed with TgAPH-specific antibodies (red) confirm APH loss following 48 hr rapamycin treatment and concurrent gain of YFP in ty-APH-LoxP parasites. Bottom: In ty-APH-cKO parasites, ablation of TgAPH (indicated by the presence of YFP) had no effect on the localization of other micronemal proteins as indicated by correct MIC4 localization. Scale bar 2 μm unless otherwise stated.

(B and C) Parasites lacking TgAPH (ty-APH-cKO) are significantly impaired in (B) invasion and (C) egress. Red (GAP45): total parasites. YFP: parasites lacking TgAPH. Error bars represent ±SD for 50 vacuoles/cells counted in triplicate from six biological replicates.

(D) Western blot analyses demonstrate the absence of TgAPH protein in the ty-APH-cKD line in the presence of ATc (48 hr). Profilin (PRF); loading control.

(E) Plaque formation was impaired for TgAPH-depleted parasites (ty-APH-cKD +ATc) but not parental lines (ty-APH-cKD -ATc/TATi-1 ± ATc).

(F) Tachyzoites depleted in TgAPH (ty-APH-cKD +ATc), but not wild-type ΔKU80 parasites, were impaired in egress. Results represent mean ± SD of 100 vacuoles counted in triplicate from three biological replicates.

(G) ty-APH-cKD parasites are unable to secrete their micronemes as indicated by the absence of signal when ESA was probed for various MICs. ESA: excreted secretory antigens/microneme secreted fraction. Red arrowhead: secreted MIC. –: full-length protein. GRA1; control for parasite viability. Catalase; control for parasite lysis.

Upon ATc treatment, ty-APH-cKD was efficiently depleted (Figure 5D) and exhibited abrogated lysis plaque formation (Figure 5E), impaired invasion (Figure S3K), and a block in egress (Figure 5F), thus confirming the ty-APH-cKO phenotype (Figures 5A–5C). Importantly, ATc-treated ty-APH-cKD parasites (Figure 5G, right panels) but not untreated (Figure 5G, left panels) or TATi-1 parental parasites (Figure S3L) failed to secrete their micronemes when stimulated with A23187, ethanol, or propranolol, demonstrating that TgAPH is indeed essential for microneme exocytosis.

CONCLUSIONS

Previous studies have indirectly shown the importance of the PI-PLC pathway during microneme secretion signaling by focusing on the production of Ca^{2+} (Carruthers et al., 1999; Lovett et al., 2002; Raabe et al., 2011) and the subsequent CDPK-dependent signaling cascade culminating in microneme exocytosis (Lourido et al., 2012; McCoy et al., 2012; reviewed in Holder et al., 2012; Garrison et al., 2012). Here we have delved into the importance of DAG and PA generated by PI-PLC during this signaling cascade. Importantly, we have directly linked these specific signaling events to the microneme surface protein: APH, which is essential for microneme secretion, invasion, and egress. This function is likely conserved across the phylum, since APH is found in all apicomplexan parasites characterized to date (Figure S3B), including the less well studied *Theileria spp*. and *Babesia spp*., which also contain micronemes (Rudzinska et al., 1976; Schein et al., 1978). We propose that following specific external stimuli such as changing potassium levels, PI-PLC activity is upregulated to produce more DAG, which is in turn converted to PA by DGK1. Concurrently, PI-PLC-generated IP_3

liposome bound proteins; fractions 3–5 contain unbound proteins. Immunoblots were probed with rabbit anti-APH or myc antibodies. Blots are representative of three replicate experiments.

(G) Quantification of liposome binding assays. p values generated from Student's t test. *$p < 0.05$; **$p < 0.01$. Error bars represent ±SD from three biological replicates.

(H) Extracellular DDmyc-APH parasites treated with extracellular buffer (EC) in the presence/absence of 30 μM R59022 or 200 μM propranolol. DDmyc-APH relocalizes to the parasite apex in the presence of propranolol, but this is ablated by addition of R59022. Scale bar: 1 μm.

(I) Quantification of DDmyc-APH relocalization upon propranolol treatment. Error bars represent ±SD for 100 cells counted in triplicate from three biological replicates.

stimulates Ca^{2+} release, leading to CDPK activation. These events culminate in microneme fusion at the PPM, which is presumably enacted initially by APH binding to PA, ultimately facilitating the close apposition of the microneme to the PPM, DOC2.1 fusion, and eventually microneme exocytosis (Figure 1A).

While these data reveal the importance of APH and PA during microneme secretion, they also reveal the importance of DAG/PA regulation during membrane signaling and homeostasis. Given the constitutive presence of low-level PA at the PPM, as indicated by $Spo20p_{wt}$ labeling, it is not surprising that conditional depletion of DGK1 or PI-PLC has a significant effect on overall parasite fitness. In other systems, DGK knockdown has been linked to apoptosis via lipid deregulation (Huang and Freter, 2015; Tsuchiya et al., 2015); thus, such an extreme phenotype upon PI-PLC or DGK1 depletion is to be expected and suggests that both PI-PLC and DGK1 functioning is important for maintaining diverse membrane signaling events not limited to microneme exocytosis. Such a role fits with the slight changes seen in PA levels detected upon DGK1 depletion. Furthermore, the conservation of DGK1 across the Apicomplexa (Figure S1) and its relatively weak homology with its mammalian counterpart make it an ideal candidate for anti-parasitic intervention strategies.

DAG/PA generation is a reversible process, and we propose that the rapid conversion of PA back to DAG acts as the "off switch" during microneme secretion-dependent events such as gliding. This is supported by the effect of propranolol that indicates that blocking PAP activity with this compound prevents multiple independent rounds of secretion and promotes one single, large burst of microneme exocytosis (Figure 1G), thus overriding the "off switch." The putative enzyme underpinning this step in *T. gondii* (PAP2, ToxoDB: TGME49_247360) (Figure S4) is not conserved across the Apicomplexa and is only present within the coccidian subgroup of the phylum (http://toxodb.org/toxo/; Figure S4A); thus, additional PAPs may be involved in PA/DAG conversion throughout the phylum. Additionally, knockdown of TgPAP2 using the recently developed 3′ UTR excision strategy (Pieperhoff et al., 2015) revealed no significant lytic cycle defect, suggesting that this protein is either not essential or only a small amount (such as that remaining following knockdown) is required for maintaining PA/DAG homeostasis (Figures S4B–S4H). Other putative candidates for PAP functioning do however also exist within the Apicomplexa (Figure S4), and one of these other candidates could instead fulfil the role; however, this remains to be experimentally validated. In addition, other members of the Apicomplexa, such as *Plasmodium* merozoites, might not necessarily need to "turn off" microneme secretion while moving between host cells, and thus PAP activity is not necessarily an absolute requirement across the entire phylum. The significant phenotype generated by conditional depletion of *Tgdgk1*, and its conservation across the phylum, does however position it as a far more central target in the development of intervention strategies and thus of significantly greater importance.

In conclusion, the conservation of both DGK1 and APH, combined with data indicating that both PfAPH and TgAPH specifically bind PA and TgAPH localizes to the micronemes, strongly suggests that the pathway identified here is likely conserved across the phylum. These findings therefore greatly enhance our understanding of the signaling events underpinning apicomplexan microneme exocytosis and provide data on not solely the signaling events but also the protein sensors involved. Importantly, DGK1 and PI-PLC have been linked here to broader roles than purely enacting microneme exocytosis and ultimately highlight DGK1 as an apicomplexan-specific drug target underpinning essential lipid signaling-related events in this important group of pathogens.

EXPERIMENTAL PROCEDURES

Antibodies

Rabbit anti-APH, rabbit anti-GAP45 (Plattner et al., 2008), mouse anti-Ty (BB2), mouse anti-Myc (mAb9E10), mouse anti-MIC2, mouse anti-SAG1, mouse anti-GRA1 (Sibley et al., 1995), rabbit anti-ARO (Mueller et al., 2013), rabbit anti-Catalase (Ding et al., 2000), and rabbit anti-Profilin (also used for GST-detection in PIP-strip assays) (Plattner et al., 2008).

Proteinase K Protection Assay

Freshly egressed *T. gondii* tachyzoites were resuspended in 1.5 ml cold SoTE (0.6 M sorbitol, 20 mM Tris–HCl [pH 7.5], and 2 mM EDTA) and split into three tubes (0.5 ml each). Cold SoTE was added to tube 1 as a control. Tubes 2 and 3 were permeabilized with 0.5 ml cold 0.01% digitonin (Sigma)/SoTE. Samples were carefully mixed by inversion and incubated on ice/10 min prior to centrifugation (2,000 × *g*/4°C/10 min). Supernatant was discarded, and 0.5 ml cold SoTE was added to tube 1, while 2.25 μl of cold Proteinase K (Sigma, 20 mg/ml)/SoTE was added to tube 3. All tubes were gently inverted and incubated on ice/30 min. Proteinase K was inactivated by addition of cold trichloroacetic acid to a final concentration of 10% on ice/30 min. Samples were centrifuged (14,000 rpm/20 min), washed 2× with acetone, air dried, and resuspended in TE prior to SDS–PAGE.

IFA

HFF monolayers grown on coverslips were inoculated with tachyzoites and grown at 37°C. Cells were subsequently fixed with 4% paraformaldehyde (PFA) or 4% PFA/0.05% glutaraldehyde (PAF/Glu) for 10 min, then quenched with 0.1 M glycine/PBS. Cells were permeabilized (0.2% Triton X-100/PBS), blocked (2% BSA/0.2%Triton/PBS), and probed with primary antibodies (60 min) prior to washing (0.2%Triton/PBS) and incubation with secondary antibodies (Alexa488- or Alexa594-conjugated goat anti-mouse/rabbit). Nuclei were stained with DAPI, and coverslips were mounted in FluoromountG. Image analysis was done using an LSM 700 confocal scanning microscope (Zeiss).

Microneme Secretion Assay

Freshly egressed parasites were resuspended in equal volume intracellular (IC) buffer (5 mM NaCl, 142 mM KCl, 1 mM $MgCl_2$, 2 mM EGTA, 5.6 mM glucose, 25 mM HEPES, pH to 7.2 with KOH) prior to pelleting (1,050 rpm/10 min). Pellets were subsequently washed in IC buffer and re-pelleted before resuspension in serum-free media with listed pre-treatment compounds for 30 min/room temperature (RT). After pre-treatment, parasites were pelleted and resuspended in serum-free medium and DMSO, 500 μM propranolol, 2% ethanol, 500 μM zaprinast, or 3 μM A23187 (37°C/5–30 min). Parasites were pelleted (1,000 × *g*/5 min/4°C), and supernatant was transferred to new Eppendorf tubes and re-pelleted (2,000 × *g*/5 min/4°C). Final supernatant (excreted secreted antigens [ESAs]) and pellet fractions were resuspended in sample buffer (50 mM Tris-HCl [pH 6.8], 10% glycerol, 2 mM EDTA, 2% SDS, 0.05% bromophenol blue, 100 mM DTT) and boiled prior to analysis by immunoblotting.

For Figure 1F, parasites were resuspended in 100 μl IC buffer ± 500 μM propranolol (37°C/30 min). Samples were spun as above, and supernatant was collected (Intra. Figure 1F). Pellets were resuspended in 100 μl serum-free media ± 500 μM propranolol (37°C/30 min), pelleted as before, and supernatant was collected (Extra. Figure 1F). Final pellet was resuspended in 100 μl serum free medium ± 500 μM propranolol +2% ethanol, pelleted, and supernatant was collected (Extra +EtOH, Figure 1F).

Protein-Lipid Overlay Assay

PIP-strip (Echelon Biosciences) assays were carried out according to manufacturer's instructions. Briefly, strips were incubated (1 hr) in PBST/BSA (PBS, 0.1% Tween 20, 3% BSA) prior to incubation with 0.5 μg/ml of each protein for 1 hr. Strips were washed 3 × 10 min with PBS/0.1% Tween before incubation with specific antibodies for 1 hr/RT. PIP-strips were subsequently washed and probed with specific secondary antibodies.

Liposome Binding and Membrane Flotation Assay

Lipids (Avanti Polar Lipids Inc.); 1-pamitoyl-2-oleoyl-sn-glyero-3-phosphocholine (POPC), 1-pamitoyl-2-oleoyl-sn-glycero-3-phospho-L-serine (POPS), and 1-pamitoyl-2-oleoyl-sn-glycero-3-phosphate (POPA) were solubilized in chloroform, mixed, and vortexed in tubes at specific ratios (PC = 100 mol% PC; PS/PC = 50 mol% PC and 50 mol% PS; PA/PC = 50 mol% PC and 50 mol% PA). Chloroform was evaporated under N_2. Dried lipids (2 μmol) were hydrated for 30 min in 1 ml of lipid rehydration buffer (100 mM NaCl, 1 mM $CaCl_2$, and 50 mM Tris-Cl [pH 7.4]) prior to three freeze/thaw cycles and extrusion through 4 μm pore-size filters using a mini-extruder (Avanti Polar Lipids) to produce liposomes.

For binding assays, liposomes (200 nmol) were incubated with 500 pmol recombinant protein (37°C/1 hr) in a final volume of 100 μl. Reaction mixture was subsequently diluted to 200 μl with 85% sucrose, then layered with 2.8 ml 65% sucrose and 1 ml 10% sucrose, and centrifuged (115,000 × *g*/4°C/16 hr). Sucrose solutions were prepared in buffer containing 100 mM NaCl, 50 mM Tris-Cl (pH 7.4). Five 1 ml fractions were collected from the top of each tube and were analyzed by immunoblot. Band intensity was quantified using an Odyssey imaging system (Li-Cor Inc.). Liposome binding efficiency was calculated as % of bound = bound/(bound + unbound) * 100.

PA Extraction and Quantification

Total lipid spiked with 25 nmol C13:0 fatty acid was extracted by chloroform: methanol 1:2(v/v) and chloroform:methanol 2:1 (v/v) in the presence of 0.1 M HCl. The pooled organic phase was subjected to biphasic separation by adding 0.1 M HCl and was then dried under N_2 gas flux prior to being dissolved in 1-butanol. Total lipid was separated by 2D HPTLC with 1 μg PA (C17:0/C17:0, Avanti Polar lipids) using chloroform/methanol/28% NH_4OH, 60:35:8 (v/v/v) as the first dimension and chloroform/acetone/methanol/acetic acid/water, 50:20:10:13:5 (v/v/v/v/v) as the second dimension solvent system (Tanaka et al., 2012). The spot corresponding to PA (identified according to migration of authentic PA standard) was then extracted for quantification of fatty acids by GC-MS (Agilent 5977A-7890B) after methanolysis (MacRae et al., 2012). Fatty acid methyl esters were identified by their mass spectrum and retention time and quantified by the calibration curve generated by fatty acid methyl ester standards. PA content was normalized according to parasite cell number and a C13:0 internal standard.

SUPPLEMENTAL INFORMATION

Supplemental Information includes four figures, two tables, four movies, and Supplemental Experimental Procedures and can be found with this article online at http://dx.doi.org/10.1016/j.chom.2016.02.006.

AUTHOR CONTRIBUTIONS

H.E.B.: Designed and conducted experiments, wrote the paper, constructed the figures. Y.J.: Designed and conducted experiments. Y.Y.-B.: Conducted PA measurements. H.B.: Conducted experiments. O.Z.: Conducted liposome binding assays. N.K.J.: Conducted experiments. J.-B.M.: Conducted experiments. V.C.: Designed liposome binding assays. C.Y.B.: Designed & conducted PA measurements. D.S.-F.: Designed experiments and wrote the paper.

ACKNOWLEDGMENTS

This work was supported by the Swiss National Foundation (FN3100A0-116722 to D.S.-F.) and US NIH (AI46675 to V.C.). H.E.B. was supported by the Indo–Swiss joint research project (ISJRP-138850). D.S.-F. is an HHMI senior international research scholar. C.Y.B. is an ATIP-Avenir and FINOVI fellow (Project Apicolipid). C.Y.B. and Y.Y.-B. are supported by Agence Nationale de la recherche (ANR), Parafrap labex Atip-Avenir, FINOVI, and Agir-Université Joseph Fourier (Project Apicolipid). We are grateful to Chetan Chitnis for fruitful discussion. We would like to acknowledge Luis Miguel Ortega Mora for preliminary work completed with propranolol, Dr. Silvia Moreno for providing the GCaMP3 and GCaMP6f-expressing tachyzoites, and Dr. Markus Meissner for providing the (3′ UTR-SAG1-HXGPRT)-4xU1 plasmid.

Received: June 25, 2015
Revised: September 28, 2015
Accepted: February 17, 2016
Published: March 9, 2016

REFERENCES

Ammar, M.R., Kassas, N., Chasserot-Golaz, S., Bader, M.-F., and Vitale, N. (2013). Lipids in Regulated Exocytosis: What are They Doing? Front. Endocrinol. (Lausanne) *4*, 125, http://dx.doi.org/10.3389/fendo.2013.00125.

Andenmatten, N., Egarter, S., Jackson, A.J., Jullien, N., Herman, J.-P., and Meissner, M. (2013). Conditional genome engineering in Toxoplasma gondii uncovers alternative invasion mechanisms. Nat. Methods *10*, 125–127, http://dx.doi.org/10.1038/nmeth.2301.

Baron, C.L., and Malhotra, V. (2002). Role of diacylglycerol in PKD recruitment to the TGN and protein transport to the plasma membrane. Science *295*, 325–328, http://dx.doi.org/10.1126/science.1066759.

Borges-Pereira, L., Budu, A., McKnight, C.A., Moore, C.A., Vella, S.A., Hortua Triana, M.A., Liu, J., Garcia, C.R.S., Pace, D.A., and Moreno, S.N.J. (2015). Calcium Signaling throughout the Toxoplasma gondii Lytic Cycle: A STUDY USING GENETICALLY ENCODED CALCIUM INDICATORS. J. Biol. Chem. *290*, 26914–26926, http://dx.doi.org/10.1074/jbc.M115.652511.

Botté, C.Y., Dubar, F., McFadden, G.I., Maréchal, E., and Biot, C. (2012). Plasmodium falciparum apicoplast drugs: targets or off-targets? Chem. Rev. *112*, 1269–1283, http://dx.doi.org/10.1021/cr200258w.

Brochet, M., Collins, M.O., Smith, T.K., Thompson, E., Sebastian, S., Volkmann, K., Schwach, F., Chappell, L., Gomes, A.R., Berriman, M., et al. (2014). Phosphoinositide metabolism links cGMP-dependent protein kinase G to essential Ca^{2+} signals at key decision points in the life cycle of malaria parasites. PLoS Biol. *12*, e1001806, http://dx.doi.org/10.1371/journal.pbio.1001806.

Budu, A., and Garcia, C.R.S. (2012). Generation of second messengers in Plasmodium. Microbes Infect. *14*, 787–795, http://dx.doi.org/10.1016/j.micinf.2012.04.012.

Carruthers, V.B., Moreno, S.N., and Sibley, L.D. (1999). Ethanol and acetaldehyde elevate intracellular [Ca2+] and stimulate microneme discharge in Toxoplasma gondii. Biochem. J. *342*, 379–386.

Chasserot-Golaz, S., Coorssen, J.R., Meunier, F.A., and Vitale, N. (2010). Lipid dynamics in exocytosis. Cell. Mol. Neurobiol. *30*, 1335–1342, http://dx.doi.org/10.1007/s10571-010-9577-x.

de Chaffoy de Courcelles, D.C., Roevens, P., and Van Belle, H. (1985). R 59 022, a diacylglycerol kinase inhibitor. Its effect on diacylglycerol and thrombin-induced C kinase activation in the intact platelet. J. Biol. Chem. *260*, 15762–15770.

Ding, M., Clayton, C., and Soldati, D. (2000). Toxoplasma gondii catalase: are there peroxisomes in toxoplasma? J. Cell. Sci. *113* (Pt 13), 2409–2419.

Fang, J., Marchesini, N., and Moreno, S.N.J. (2006). A Toxoplasma gondii phosphoinositide phospholipase C (TgPI-PLC) with high affinity for phosphatidylinositol. Biochem. J. *394*, 417–425, http://dx.doi.org/10.1042/BJ20051393.

Farrell, A., Thirugnanam, S., Lorestani, A., Dvorin, J.D., Eidell, K.P., Ferguson, D.J.P., Anderson-White, B.R., Duraisingh, M.T., Marth, G.T., and Gubbels, M.-J. (2012). A DOC2 protein identified by mutational profiling is essential for apicomplexan parasite exocytosis. Science *335*, 218–221, http://dx.doi.org/10.1126/science.1210829.

Garg, S., Agarwal, S., Kumar, S., Yazdani, S.S., Chitnis, C.E., and Singh, S. (2013). Calcium-dependent permeabilization of erythrocytes by a perforin-like protein during egress of malaria parasites. Nat. Commun. *4*, 1736, http://dx.doi.org/10.1038/ncomms2725.

Garrison, E., Treeck, M., Ehret, E., Butz, H., Garbuz, T., Oswald, B.P., Settles, M., Boothroyd, J., and Arrizabalaga, G. (2012). A forward genetic screen reveals that calcium-dependent protein kinase 3 regulates egress in Toxoplasma. PLoS Pathog. *8*, e1003049, http://dx.doi.org/10.1371/journal.ppat.1003049.

Herm-Götz, A., Agop-Nersesian, C., Münter, S., Grimley, J.S., Wandless, T.J., Frischknecht, F., and Meissner, M. (2007). Rapid control of protein level in the apicomplexan Toxoplasma gondii. Nat. Methods *4*, 1003–1005, http://dx.doi.org/10.1038/nmeth1134.

Holder, A.A., Mohd Ridzuan, M.A., and Green, J.L. (2012). Calcium dependent protein kinase 1 and calcium fluxes in the malaria parasite. Microbes Infect. *14*, 825–830, http://dx.doi.org/10.1016/j.micinf.2012.04.006.

Huang, C., and Freter, C. (2015). Lipid metabolism, apoptosis and cancer therapy. Int. J. Mol. Sci. *16*, 924–949, http://dx.doi.org/10.3390/ijms16010924.

Jean, S., Zapata-Jenks, M.A., Farley, J.M., Tracy, E., and Mayer, D.C.G. (2014). Plasmodium falciparum double C2 domain protein, PfDOC2, binds to calcium when associated with membranes. Exp. Parasitol. *144*, 91–95, http://dx.doi.org/10.1016/j.exppara.2014.06.015.

Kooijman, E.E., Chupin, V., de Kruijff, B., and Burger, K.N.J. (2003). Modulation of membrane curvature by phosphatidic acid and lysophosphatidic acid. Traffic *4*, 162–174.

Lindner, S.E., Sartain, M.J., Hayes, K., Harupa, A., Moritz, R.L., Kappe, S.H.I., and Vaughan, A.M. (2014). Enzymes involved in plastid-targeted phosphatidic acid synthesis are essential for Plasmodium yoelii liver-stage development. Mol. Microbiol. *91*, 679–693, http://dx.doi.org/10.1111/mmi.12485.

Lourido, S., Tang, K., and Sibley, L.D. (2012). Distinct signalling pathways control Toxoplasma egress and host-cell invasion. EMBO J. *31*, 4524–4534, http://dx.doi.org/10.1038/emboj.2012.299.

Lovett, J.L., Marchesini, N., Moreno, S.N.J., and Sibley, L.D. (2002). Toxoplasma gondii microneme secretion involves intracellular Ca(2+) release from inositol 1,4,5-triphosphate (IP(3))/ryanodine-sensitive stores. J. Biol. Chem. *277*, 25870–25876, http://dx.doi.org/10.1074/jbc.M202553200.

MacRae, J.I., Sheiner, L., Nahid, A., Tonkin, C., Striepen, B., and McConville, M.J. (2012). Mitochondrial metabolism of glucose and glutamine is required for intracellular growth of Toxoplasma gondii. Cell Host Microbe *12*, 682–692, http://dx.doi.org/10.1016/j.chom.2012.09.013.

McCoy, J.M., Whitehead, L., van Dooren, G.G., and Tonkin, C.J. (2012). TgCDPK3 regulates calcium-dependent egress of Toxoplasma gondii from host cells. PLoS Pathog. *8*, e1003066, http://dx.doi.org/10.1371/journal.ppat.1003066.

Mueller, C., Klages, N., Jacot, D., Santos, J.M., Cabrera, A., Gilberger, T.W., Dubremetz, J.F., and Soldati-Favre, D. (2013). The Toxoplasma protein ARO mediates the apical positioning of rhoptry organelles, a prerequisite for host cell invasion. Cell Host Microbe *13*, 289–301.

Nakanishi, H., de los Santos, P., and Neiman, A.M. (2004). Positive and negative regulation of a SNARE protein by control of intracellular localization. Mol. Biol. Cell *15*, 1802–1815, http://dx.doi.org/10.1091/mbc.E03-11-0798.

Pieperhoff, M.S., Pall, G.S., Jiménez-Ruiz, E., Das, S., Melatti, C., Gow, M., Wong, E.H., Heng, J., Müller, S., Blackman, M.J., and Meissner, M. (2015). Conditional U1 Gene Silencing in Toxoplasma gondii. PLoS ONE *10*, e0130356, http://dx.doi.org/10.1371/journal.pone.0130356.

Plattner, F., Yarovinsky, F., Romero, S., Didry, D., Carlier, M.F., Sher, A., and Soldati-Favre, D. (2008). Toxoplasma profilin is essential for host cell invasion and TLR11-dependent induction of an interleukin-12 response. Cell Host Microbe *3*, 77–87.

Raabe, A., Berry, L., Sollelis, L., Cerdan, R., Tawk, L., Vial, H.J., Billker, O., and Wengelnik, K. (2011). Genetic and transcriptional analysis of phosphoinositide-specific phospholipase C in Plasmodium. Exp. Parasitol. *129*, 75–80, http://dx.doi.org/10.1016/j.exppara.2011.05.023.

Rudzinska, M.A., Trager, W., Lewengrub, S.J., and Gubert, E. (1976). An electron microscopic study of Babesia microti invading erythrocytes. Cell Tissue Res. *169*, 323–334.

Schein, E., Mehlhorn, H., and Warnecke, M. (1978). Electron microscopic studies on the schizogony of four *Theileria* species of cattle (*T. parva*, *T. lawrencei*, *T. annulata* and *T. mutans*). Protistologica (Paris) *XIV*, 337–348.

Sharma, P., and Chitnis, C.E. (2013). Key molecular events during host cell invasion by Apicomplexan pathogens. Curr. Opin. Microbiol. *16*, 432–437, http://dx.doi.org/10.1016/j.mib.2013.07.004.

Sibley, L.D., Niesman, I.R., Parmley, S.F., and Cesbron-Delauw, M.F. (1995). Regulated secretion of multi-lamellar vesicles leads to formation of a tubulo-vesicular network in host-cell vacuoles occupied by *Toxoplasma gondii*. J. Cell. Sci. *108* (Pt 4), 1669–1677.

Sidik, S.M., Hackett, C.G., Tran, F., Westwood, N.J., and Lourido, S. (2014). Efficient genome engineering of Toxoplasma gondii using CRISPR/Cas9. PLoS ONE *9*, e100450, http://dx.doi.org/10.1371/journal.pone.0100450.

Singh, S., and Chitnis, C.E. (2012). Signalling mechanisms involved in apical organelle discharge during host cell invasion by apicomplexan parasites. Microbes Infect. *14*, 820–824, http://dx.doi.org/10.1016/j.micinf.2012.05.007.

Singh, S., Alam, M.M., Pal-Bhowmick, I., Brzostowski, J.A., and Chitnis, C.E. (2010). Distinct external signals trigger sequential release of apical organelles during erythrocyte invasion by malaria parasites. PLoS Pathog. *6*, e1000746, http://dx.doi.org/10.1371/journal.ppat.1000746.

Tanaka, T., Kassai, A., Ohmoto, M., Morito, K., Kashiwada, Y., Takaishi, Y., Urikura, M., Morishige, J., Satouchi, K., and Tokumura, A. (2012). Quantification of phosphatidic acid in foodstuffs using a thin-layer-chromatography-imaging technique. J. Agric. Food Chem. *60*, 4156–4161, http://dx.doi.org/10.1021/jf300147y.

Tsuchiya, R., Tanaka, T., Hozumi, Y., Nakano, T., Okada, M., Topham, M.K., Iino, M., and Goto, K. (2015). Downregulation of diacylglycerol kinase ζ enhances activation of cytokine-induced NF-κB signaling pathway. Biochim. Biophys. Acta *1853*, 361–369, http://dx.doi.org/10.1016/j.bbamcr.2014.11.011.

Wiersma, H.I., Galuska, S.E., Tomley, F.M., Sibley, L.D., Liberator, P.A., and Donald, R.G.K. (2004). A role for coccidian cGMP-dependent protein kinase in motility and invasion. Int. J. Parasitol. *34*, 369–380, http://dx.doi.org/10.1016/j.ijpara.2003.11.019.